Supporting information

Extremely low resistance of Li_3PO_4 electrolyte/$Li(Ni_{0.5}Mn_{1.5})O_4$ electrode interfaces

Hideyuki Kawasoko[*,†,§], *Susumu Shiraki*[†], *Toru Suzuki*[†], *Ryota Shimizu*[‡], *and Taro Hitosugi*[†,‡]

†Advanced Institute for Material Research, Tohoku University, 2-1-1 Katahira, Aoba, Sendai, Miyagi 980-8577, Japan

‡School of Materials and Chemical Technology, Tokyo Institute of Technology, 2-12-1 Ookayama, Meguro, Tokyo 152-8550, Japan

*E-mail: hideyuki.kawasoko.b7@tohoku.ac.jp

Equivalent circuit model

The impedance spectra were analyzed based on the equivalent circuit shown in Figure S1. In this model, R_{Wire}, R_{HF} R_{MF}, and R_{LF} are the wiring resistance, the high-frequency resistance, the middle-frequency resistance, and the low-frequency resistance, respectively. The abbreviations, CP_{HF}, CP_{MF}, and CP_{LF}, indicate constant phase elements of the high-frequency, middle-frequency, and the low-frequency regions, respectively. The fitting was performed in the frequency region between 6×10^0 and 1×10^5 Hz.

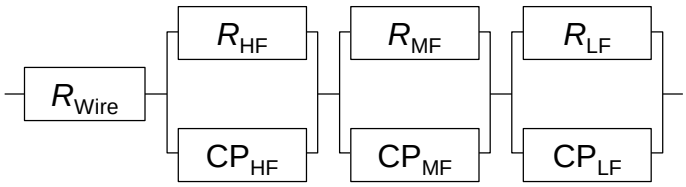

Figure S1. Equivalent circuit model for the analysis of impedance spectra.

Crystal structure analysis of $LiNi_{0.5}Mn_{1.5}O_4/LaNiO_3$ epitaxial thin films, which displayed excellent charging and discharging characteristics.

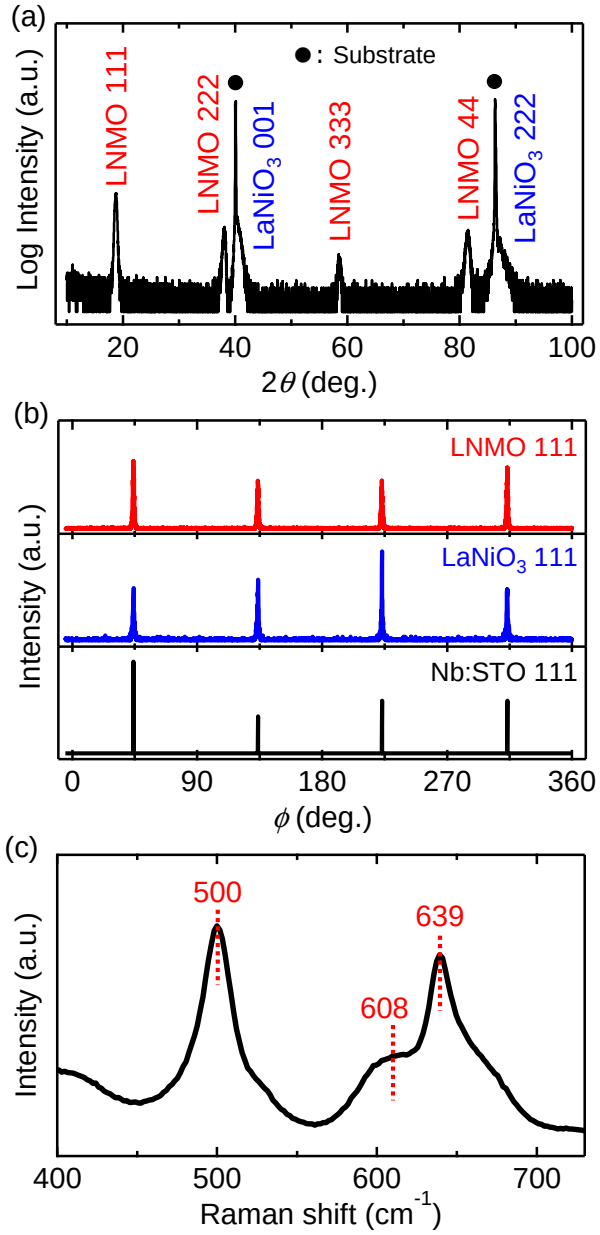

Figure S2. (a) In-plane X-ray diffraction pattern, (b) ϕ-scan, and (c) Raman spectrum of an $LiNi_{0.5}Mn_{1.5}O_4$ (LNMO)/$LaNiO_3$ thin film.

Estimation of activation energy

The E_a values were derived from the temperature dependence of the resistance components in the electrochemical impedance spectra with the use of the following Arrhenius equation:

$$\Sigma T = A\exp(-\frac{E_a}{kT}),$$

where Σ, T, A, and k are the resistance parameters (σ_{LPO}, $1/R_i$, and $1/R_{LNMO}$), the absolute temperature, the pre-exponential factor, and the Boltzmann constant, respectively. These values were estimated from electrochemical impedance spectra at 4.7 V (vs. Li^+/Li) in the temperature range between 27 and 79 °C.

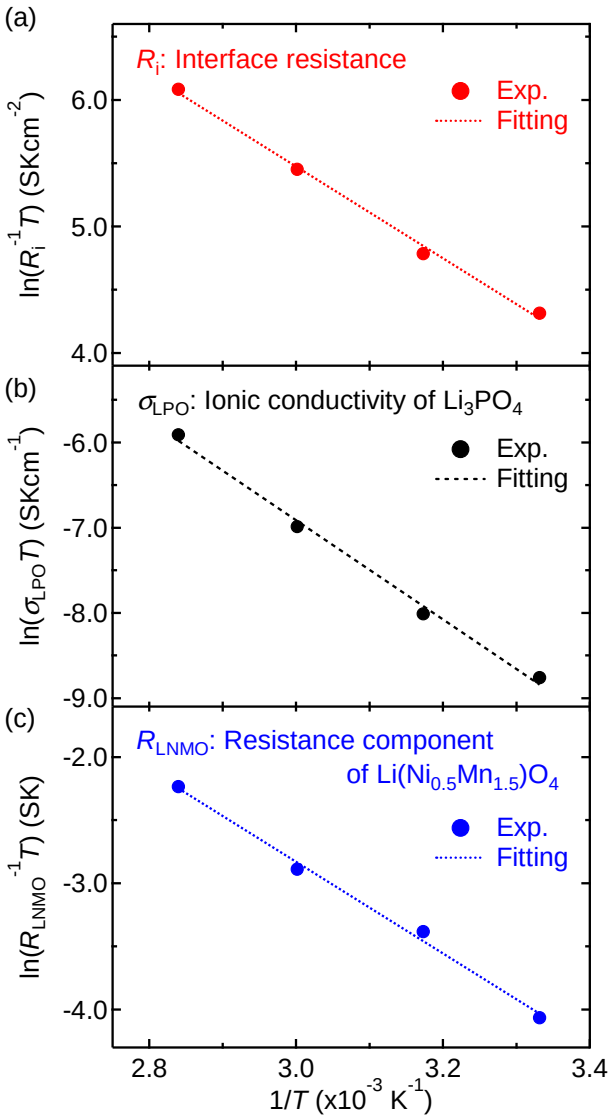

Figure S3. Temperature dependence of (a) interface resistance, (b) ionic conductivity of Li_3PO_4, and (c) resistance component of $LiNi_{0.5}Mn_{1.5}O_4$ in fabricated lithium batteries.

Battery performance of the fabricated thin-film Li batteries at 27 °C

Figure S4a and S4b show charge–discharge curves and rate capability, respectively, which were cycled at various current density from 0.0039 (1C) to 3.9 mA/cm^2 (1000C) between potentials of 3.2 and 4.8 V. Both the charge and discharge curves at 1 and 10C featured double plateaus at 4.7 V and a minor plateau at 4.0 V, which were attributed to Ni^{2+}/Ni^{4+} and Mn^{3+}/Mn^{4+} redox reactions, respectively. These charging and discharging characteristics were consistent with the results of CV measurements. At higher rates, the initial-state potential of the charge and discharge changed owing to the internal resistance of the thin-film LBs, and reduced the capacity of the LBs from 96 mA h/g at 0.039 mA/cm^2 (1C) to 1.8 mA h/g at 3.9 mA/cm^2 (1000C). At all rates, the Coulombic efficiency was approximately 100%, indicating that the fabricated LBs showed good reversibility. Furthermore, the LBs regained their capacity at 0.039 mA/cm^2 (1C) after charging and discharging at 3.9 mA/cm^2 (1000C), suggesting that the large current density—namely, fast Li-ion insertion/extraction—did not damage the solid-electrolyte/electrode interface or the crystal structure of LNMO.

Figure S4c shows the discharge capacity at various discharge rates, charging batteries in 0.039 mA/cm^2 (1C) with potentials controlled from 3.8 to 4.8 V at 27 °C. As the discharge rate increased, the double plateau region near 4.7 V shrank, indicating that the batteries were not fully discharged at these higher rates. In addition, the potential of the discharge initial state dropped owing to the internal resistance of the thin-film LBs. The discharge capacity decreased from 102 mA h/g at 0.039 mA/cm^2 (1C) to 68 mA h/g at 3.9 mA/cm^2 (1000C). Further increasing the discharge rate to 14 mA/cm^2 (3600C), decreased the discharge capacity to 0.10 mA h/g.

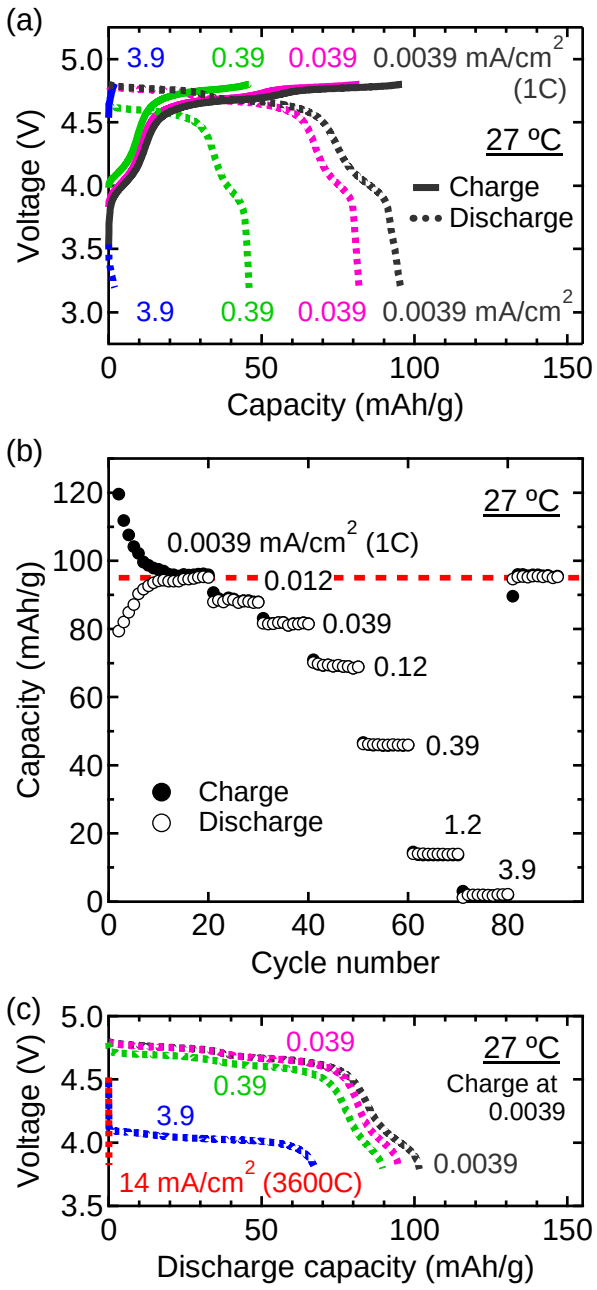

Figure S4. (a) Charge-discharge curves and (b) Rate capability at 27 °C. (c) Rate dependence of discharge curves at 27 °C.